JACS
JOURNAL OF THE AMERICAN CHEMICAL SOCIETY

ARTICLE

pubs.acs.org/JACS

Imaging Translational and Rotational Diffusion of Single Anisotropic Nanoparticles with Planar Illumination Microscopy

Lehui Xiao, Yanxia Qiao, Yan He,* and Edward S. Yeung

College of Chemistry and Chemical Engineering, College of Biology, State Key Laboratory of Chemo/Biosensing and Chemometrics, Hunan University, Changsha 410082, P. R. China

Supporting Information

ABSTRACT: Here we demonstrated a simple yet powerful method, planar illumination microscopy, to directly track the rotational and translational diffusion dynamics of individual anisotropic nanoparticles in solution and living cells. By illuminating gold nanorods (GNRs) with two orthogonal sheets of light and resolving the polarized scattering signal with a birefringent crystal, we readily achieved three-dimensional angular resolving capability for single GNRs in noisy surroundings. The rotational dynamics of individual GNRs dispersed in glycerol/water mixtures with different chemical modification were tracked, and the measured rotational diffusion coefficient was well fitted to a previously reported theoretical model (Torre, J. G. d. l.; Martinez, M. C. L. *Macromolecules* **1987**, *20*, 661−666; Tirado, M. M.; Torre, J. G. d. l. *J. Chem. Phys.* **1980**, *73*, 1986−1993). In addition, the translational and rotational movements of individual GNRs transported by kinesin motor protein on microtubules inside living cells were directly imaged. Compared to its motion in free solution, a GNR attached to motor-protein did not rotate significantly while moving forward. Our method can be further generalized to allow determination of three-dimensional orientation of single dipoles using many different illumination modes.

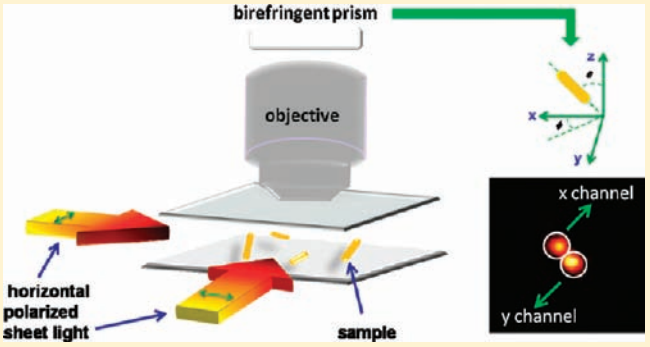

INTRODUCTION

As dynamic mechanisms embedded in nanoscopic systems are usually correlated with conformational variations, for example, the stepping process of motor proteins[3,4] and the heterogeneous glassy state of polymers,[5,6] there is an urgent need to develop convenient methods to directly follow these structural changes in real time. So far, several techniques have been reported that have the capability to reveal the rotational dynamics of macromolecules in bulk solution, including fluorescence anisotropy, depolarized light scattering, transient electric birefringence, and so forth.[7] These ensemble sampling methods only provide averaged information whereby certain important rare events are lost. In contrast, single-molecule imaging enables the unique dynamics of individual probes in their nanoenvironments to be directly monitored, providing clear information on uncorrelated motions.[5,8,9]

Until now, the most commonly used single-molecule method to explore the local order or conformational variation is fluorescence polarization imaging.[10−12] This method utilizes dyes as orientation probes because they possess well-defined transition dipoles with respect to their structures. A wealth of rotational information could be extracted from the real-time single-molecule fluorescence anisotropy trajectory, for example, the chemomechanical mechanism of F_1-ATPase[13] and the rotation jumps of individual dye molecules on cover glass.[14,15] Since most of these investigations are based on organic probes, irreversible photobleaching of the molecules limits long-time observations and results in decreased measurement accuracy. Furthermore, the labeling of a dye molecule to a large macromolecule through a single tether usually retains free rotation of the former that is independent of the rotation dynamics of the latter.[16] Although some improvement is possible through labeling with semiconductor quantum dots,[16] the complicated transition between the on and off states that causes blinking also confuses the observations. More importantly, such labels have been demonstrated to be cytotoxic to biological organisms, greatly limiting their in vivo applications.[17]

One of the solutions to these issues is to replace the fluorescent molecules with optically and chemically stable plasmon resonant nanoparticles.[18−20] The collective oscillations of the conduction band electrons on the surface of noble metal nanoparticles produce several orders of magnitude higher absorption and scattering cross sections in comparison with dye molecules.[21] Therefore, faster sampling frequency for transient dynamic processes and much better spatial localization accuracy can be achieved when using plasmon resonant nanoparticles as the contrast agents.[22−24] In particular, it has been demonstrated

Received: April 22, 2011
Published: June 16, 2011

that the absorption and scattering light from anisotropic GNRs is strongly polarized along its long axis, making GNRs in principle a perfect orientation probe instead of dye molecules.[25,26] Recently, a few optical imaging methods have been demonstrated with the capability to decipher the orientation of GNRs in situ, such as polarization detection with conventional darkfield microscopy,[27] photothermal orientation imaging,[28] and high-order coherent mode illumination with confocal microscopy.[29] However, these methods are restricted to in-plane only angle determination, low temporal resolution, and reduced spatial localization accuracy, respectively.

The motion of nanomachines or protein molecules is not always confined to two dimensions; therefore, the polar angle of the object should represent a vital parameter to elucidate kinetic mechanisms. Recently, we have demonstrated an approach to decipher the full 3D geometry information of individual GNRs with defocused darkfield microscopy.[30] Wang, et al. demonstrated another approach based on differential interference contrast (DIC) microscopy.[31] There, in principle, the angular information can be inferred from the relative intensity ratios of the dark or bright portions of the DIC diffraction pattern between the corresponding maximum values. However, that approach is not suited for imaging or tracking objects in strongly scattering media, such as inside living cells, due to typically low signal-to-noise ratio (S/N) and difficulties in discriminating the probes from other particles even with adequate S/N. In addition, the relative intensity ratio (contrast) of the DIC image is not only dependent on the orientation of GNRs, but is also affected by bias retardation and by the angle between the polarizer and the analyzer. Although introduction of a slight bias retardation can generate better contrast in noisy surroundings, it will result in additional phase delay between extraordinary and ordinary wavefronts. Therefore, experimental artifacts could be introduced in quantitatively deconvoluting the angles of GNRs from DIC results. Herein, we present a convenient method to directly decipher the three-dimensional orientation of individual GNRs in solution or inside living cells with planar illumination. This is achieved by illuminating the sample with two orthogonal sheets of light and resolving the polarization component of the scattering signal with a birefringent crystal. With this illumination mode, the excitation probability function for GNRs could be described with a simple continuous function that is a great improvement in comparison with conventional darkfield microscopy. Thanks to the large scattering cross-section and characteristic resonant frequency from GNRs, we can readily track and discriminate the probe from noisy surroundings. In addition, not only can rotational information be readily deduced but also translational diffusion information can be simultaneously determined. This is in contrast to DIC where subdiffraction positional information cannot be inferred due to the continuously changing point spreading function for rotating anisotropic nanoparticles. Applications of this approach to rheology or biology should shed light on the fundamental mechanisms about motions at nanoscopic dimensions.

RESULTS AND DISCUSSION

GNR Being a Single Dipole. The GNRs used in this study were fabricated via a seed mediated approach with a mean width of 36 ± 3 nm and a mean length of 67 ± 6 nm (Supporting Information Figure S1). Procedures for GNR preparation and other experimental details are described in the Supporting Information. Previous theoretical consideration has confirmed that the oscillation of the conductive band electrons on the surface of GNRs can be simplified into three orthogonal oscillation dipoles.[21] Oscillation along the long principal axis is the longitudinal mode, and the other two are transverse modes that vibrate along the short axes. The contribution from each component is dependent on the excitation light polarization direction, the illumination light frequency, and the physical geometry of the nanoparticle (i.e., the aspect ratio of the GNR). When the aspect ratio of the GNR deviates from one, the strength of the scattered light from the longitudinal mode is several times larger than that from the transverse one.[30] Figure 1 illustrates the measured longitudinal and transverse scattering spectra from a single GNR immersed in water on a cover glass surface through inserting a transmission grating and a birefringent beam splitter into the detection light path of a conventional darkfield microscope.[11,32] The former allows one to locate the scattering maximum without the use of optical filters (dispersed horizontally in Supporting Information Figure S2), and the latter allows one to separate the two polarizations (displaced vertically in Figure S2) while imaging on the same CCD camera. Alternatively, the two polarizations can also be separated by a dual-view attachment to typical microscopes with perpendicular polarization analyzers. The resonance frequency from the longitudinal mode with central peak at 630 nm is obviously red-shifted compared with that of the transverse mode at 530 nm. In addition, we note that the measured scattering intensity from the longitudinal oscillation is about 10 times larger than that of the transverse oscillation when using halogen lamp illumination. It means that the GNRs studied here could be simplified to a single oscillation dipole with direction along its principal axis by suppressing the contributions from transverse oscillations such as by illuminating at the longitudinal oscillation frequency or by intensity discrimination (Supporting Information Figure S3).

Detection Theory. It is well-known that the time-averaged Poynting vector measured with a far-field optical microscope from a single scattering oscillation dipole can be generally described as $I_s \propto KP_aP_s$, where K is a system parameter (constant) that is independent of the rotation dynamics of the GNR, and P_a reflects the excitation probability of the dipole which is a function of the angle between the axis of the absorption dipole and the direction of the external electric field.[7] If the oscillation dipole is evenly excited (e.g., by illuminating the sample with two orthogonal sheets of unpolarized light; Figure 1c and Supporting Information), P_a equals to one. P_s describes the detection probability function for the scattering signal from the GNR. By using a birefringent beam splitting prism (this work) or a dual-view attachment,[11] this probability function can be simplified into two components with polarization directions parallel and perpendicular to the optical axis of the prism

$$P_{sx} \propto c_1 \sin^2\theta \cos^2\varphi + c_2 \sin^2\theta \sin^2\varphi + c_3 \cos^2\theta$$

and

$$P_{sy} \propto c_2 \sin^2\theta \cos^2\varphi + c_1 \sin^2\theta \sin^2\varphi + c_3 \cos^2\theta$$

where θ is the polar angle, φ is the azimuthal angle, and c_1, c_2, and c_3 are correction factors accounting for the collimation property of the high NA value of the objective.[33] In our imaging system (with a 40× objective with NA = 0.75), c_1, c_2, and c_3 are

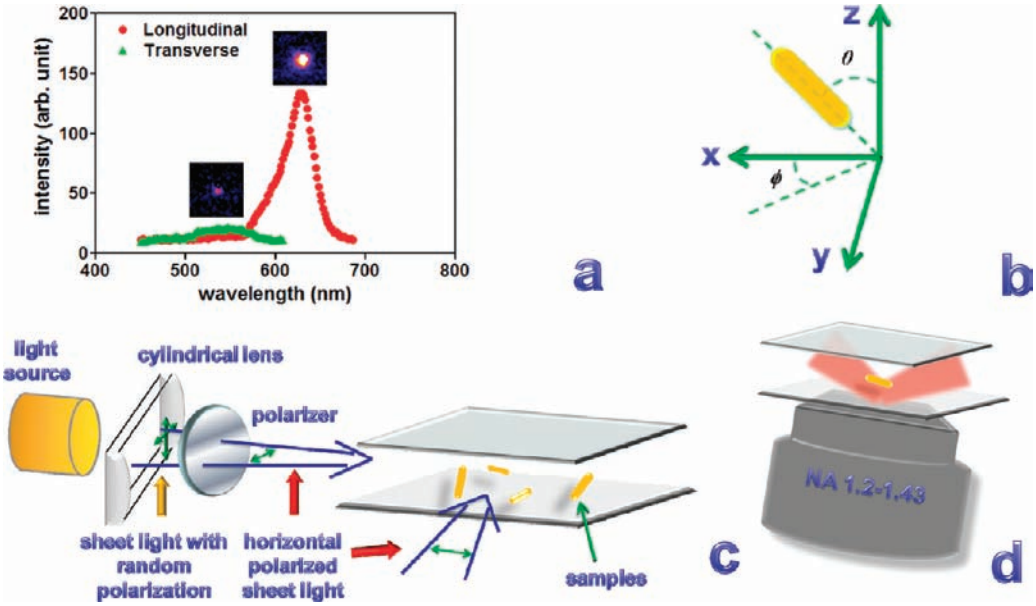

Figure 1. (a) Measured longitudinal and transverse oscillation scattering spectra of an individual GNR, obtained via inserting a transmission grating into the detection light path. Longitudinal (red) and transverse oscillation (green) components are discriminated by a birefringent beam splitter under high illumination intensity. Inset images are their corresponding scattering images. (b) Coordinate system of one GNR rotating in 3D with respect to the laboratory frame ($X-Y-Z$). Here the optical axis of the beam splitter is defined to be parallel with the X direction. (c) Light path for planar illumination (two orthogonal beams from both X and Y directions, only one is shown here for clarity). (d) Light path for conventional darkfield imaging.

determined to be 0.93, 0.00087, and 0.069, respectively (see the Supporting Information). These results approach the small aperture limit described by Axelrod,[7,33] where $c_1 \gg c_2, c_3$. Then, P_{sx} and P_{sy} can be simplified to the uncorrected equations $P_{sx} \propto \sin^2\theta \cos^2\varphi$ and $P_{sy} \propto \sin^2\theta \sin^2\varphi$. Consequently, the polar and azimuthal angle of the GNR could be readily determined through the sum intensity value between the s and p channels and the polarization factor $R = (I_{sx} - I_{sy})/(I_{sx} + I_{sy}) \approx \cos(2\varphi)$, respectively.

One more quantity that needs to be considered is the angular determination accuracy for the Z direction. For certain biological process such as the motion of motor proteins on microtubules, the structural variation usually takes place in a plane with small fluctuations in the perpendicular direction. In other words, the polar angle is commonly very large. To monitor these processes in detail, it requires a relatively high determination accuracy in the Z direction. The polar angle determination accuracy of our imaging configuration was estimated with an intensity measurement standard deviation of 1% (Supporting Information Figure S4). From this curve, we note that the accuracy is not satisfactory when the GNR is rotating with a small in-plane tilt angle. This is an inherent feature of the projection of the major axis of the GNR onto the $x-y$ plane. To further increase the polar angle determination accuracy in such systems, we introduced a polarizer behind the cylindrical lens so that we obtained $P_a \propto \sin^2\theta$ (see the Supporting Information). Compared to the determination accuracy without a polarizer, the precision is further improved especially in the large polar angle range as indicated in Figure S4. Note that, under conventional darkfield illumination mode, the excitation light is confined to a hollow circular structure with polar angles between 53° and 71°. Therefore, GNRs perpendicular to this region can be evenly excited with P_a equals to 1. However, when the angle of the oscillation dipole deviates from that range, the excitation probability function would be uncertain and varies with the projection of the electric field vector along the direction of the oscillation dipole. Thus one cannot extract accurate full three-dimensional angular information by using the light path of a conventional darkfield microscope.

Deciphering Three-Dimensional Rotational Diffusion in Solution. As a proof of concept, we studied the rotational dynamics of individual GNRs suspended in glycerol solution. Figure 2a shows 30 consecutive images of an individual CTAB-protected GNR in glycerol solution. A typical intensity trace of the CTAB-protected GNR as a function of time with a sampling frequency of 16 Hz is shown in Figure 3a. As the GNR rotates randomly in all three dimensions in glycerol, the scattering signal from each channel varies between a maximum and a minimum that is reminiscent of the blinking trajectory of fluorescent molecules. The trace of the sum value from these two channels also shows similar features in accordance with the above simplification, indicating the expected random diffusion in three dimensions. The blinking phenomenon in the intensity track indicates that the sampling frequency is adequate to capture the free rotational dynamics of CTAB protected GNRs in glycerol. Translational diffusion induced intensity fluctuations can be ruled out here because, according to the Tirado and Garcia dela Torre (TT) model,[1,2] the theoretical one-dimensional diffusion displacements for GNRs under this sampling frequency are about 0.02, 0.05, and 0.1 μm in 100%, 90%, and 80% glycerol/water mixtures, respectively, and is smaller than the depth-of-field of our imaging system of 2.0 μm (see the Supporting Information). Real-time single-particle tracking experiments also confirmed this point as shown in the scatter plot of displacements in the X and Y directions (Figure 3c). The well focused image of the GNR during the entire observation period further supports this argument. It is noteworthy that the translational motion of the GNR is nearly frozen in the glycerol solution as indicated by the narrow

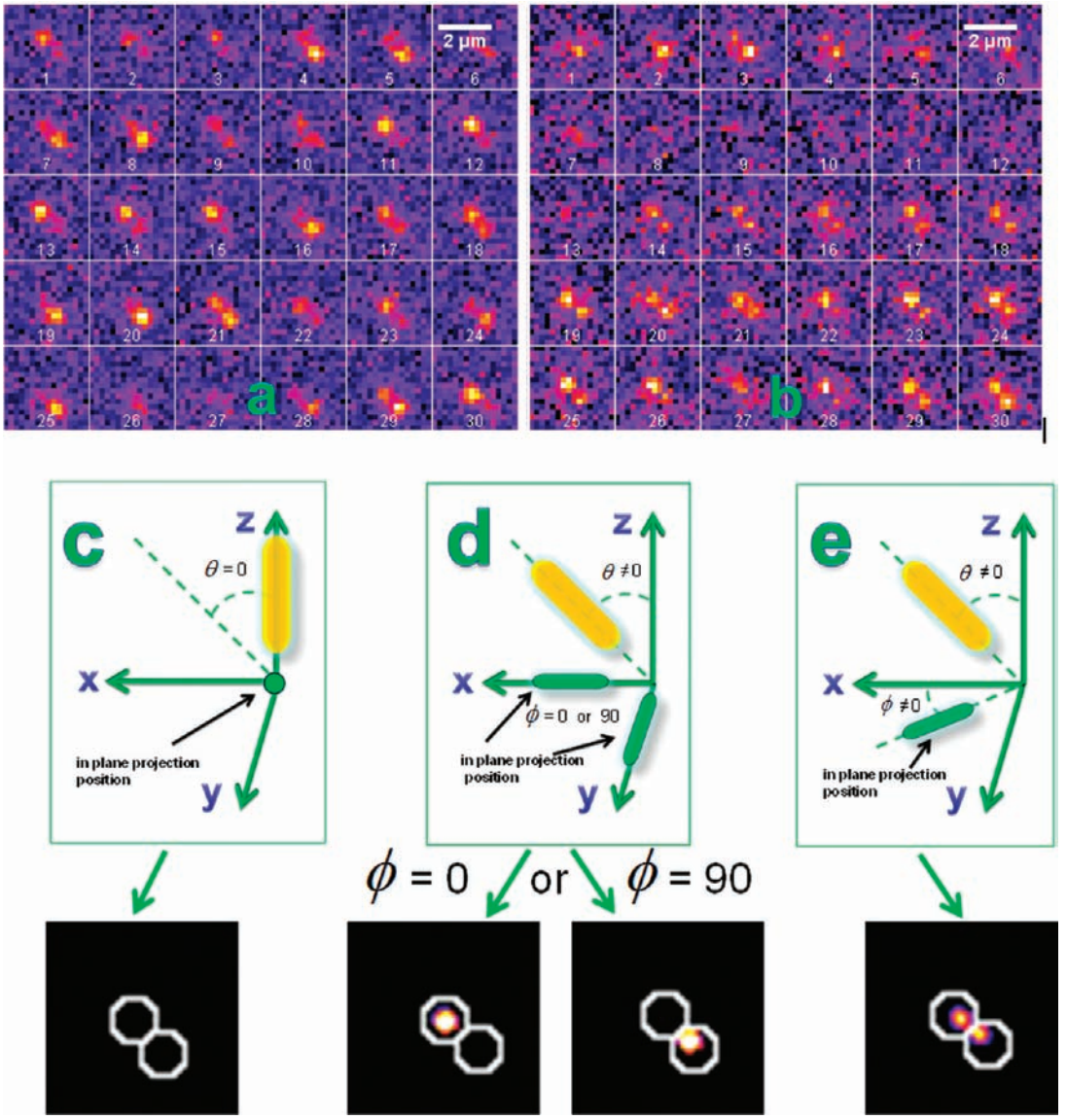

Figure 2. Montage images of an individual GNR from 30 consecutive frames dispersed in 100% glycerol solution with CTAB (a) and SH-PEG (b) modification. Translational diffusions are nearly frozen while the rotational diffusions are still vigorous. The rotation rate of the CTAB modified GNR is obviously faster than that of the SH-PEG modified GNR (see the intensity variation between two channels). When the signals from both channels vanish, the long axis of the GNR is parallel to observation direction (*Z* axis, see the 3D coordinate scheme and the corresponding schematic drawing in (c)). If only one dot appears, the long axis of the GNR is parallel to either the *XZ* or *YZ* plane (d). When both of the dots appear, the long axis of the GNR has nonzero angles between *X*, *Y*, and *Z* axes (e).

fluctuations in the displacement pattern in Figure 3c. When observing the rotational motion of GNRs with conventional darkfield microscopy, a similar blinking trace from the sum value could also be obtained. However, it is impossible to deduce the polar angle from that detection configuration due to the complicated excitation probability function as discussed above. The measured rotational diffusion constant (through calculating the autocorrelation decay time constant $\tau = 1/6D_r$)[27] of CTAB protected GNRs in 100% glycerol solution is $4.6 \pm 3.1\ s^{-1}$ which is in agreement with the value of $3.3\ s^{-1}$ as determined by the TT model.

To study the surface chemistry effect on the rotational dynamics of GNRs, thiolated PEG with a molecular weight of 5000 g/mol was covalently attached onto the GNR surface. Figure 3b clearly shows slower rotational diffusion in comparison with that of the CTAB-protected GNR. Detailed step-by-step random rotation in 100% glycerol could be easily followed in contrast to the CTAB-modified GNR (see Figure 2b and Movie 1 in the Supporting Information, individual GNRs are highlighted by white circles in the movie). The measured rotational diffusion constant of PEG protected GNRs is about 1/7 of that of CTAB-modified GNRs. This result is reasonable because the rotational diffusion of anisotropic nanoparticles is very sensitive to the frictional force between its side wall and the surrounding medium.[34,35] Due to the long carbon chain of the PEG molecule, van de Waals and hydrophilic interactions between GNRs and glycerol molecules should be greatly increased. This is similar to the results reported by Pierrat et al. where the chemical properties of the ligand molecule play a significant role in controlling the rotational motion of GNRs.[36] Therefore, when using long-chain

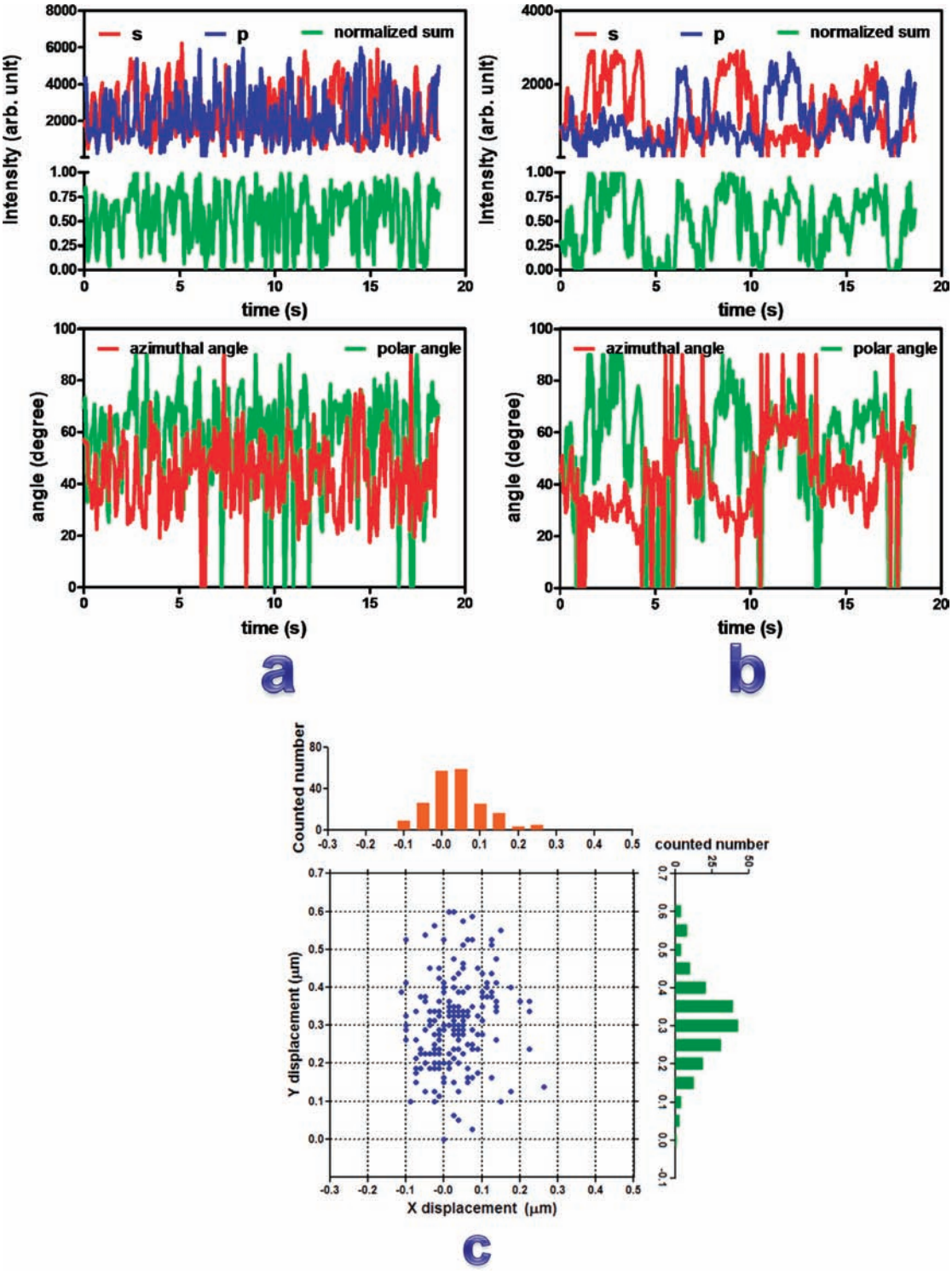

Figure 3. (a) Measured scattering signal from s (red) and p (blue) channel and the normalized sum value (green) of a CTAB protected GNR dispersed in 100% glycerol (upper panel). The plot in the lower panel is the corresponding measured polar (green) and azimuthal (red) angle of the GNR as a function of time. Similar results from a PEG modified GNR dispersed in 100% glycerol are shown in (b). (c) Scatter plot of relative displacements in the *X* and *Y* directions within 12 s from the CTAB protected GNR dispersed in 100% glycerol. The corresponding frequency histograms at *X* and *Y* directions represent a Gaussian distribution where random walk is expected.

modified nanoparticles, the frictional force needs to be carefully corrected for.

Real Time Monitoring of Rotational and Translational Diffusion in Living Cells. To demonstrate the applicability of our technique to biological systems, we explored the rotational and translational diffusion dynamics of GNRs inside a living cell. Due to the randomness of in vivo single-particle tracking, it requires monitoring the probe over a relatively long time span.

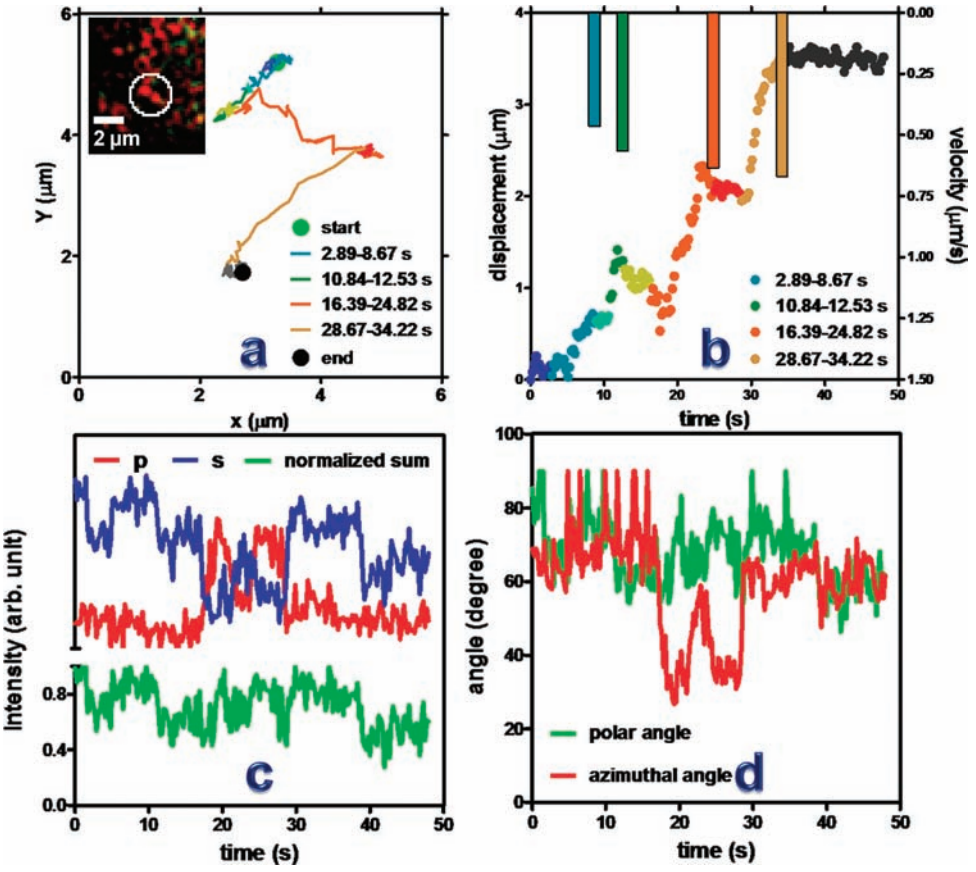

Figure 4. (a) Trajectory of a GNR stepping on microtubule with kinesin motor protein inside a living cell. Forward steps are highlighted with different colors as indicated in the inset text. To make sure the observed spot is from the GNR, a color CCD image is shown in the inset picture (highlighted by white circle). (b) Relative displacement of the GNR as a function of time (dotted curve) and corresponding velocities at each forward step (color bar). (c) Scattering intensity from *X* (red) and *Y* (blue) channel and normalized sum value (green). (d) Measured polar and azimuthal angle of the GNR.

This requires the probe to show high photophysical and chemical stability under high salt conditions. In addition, since the optical properties of plasmonic nanoparticles will be significantly changed once dimers, trimers, or even oligomers are formed, we need to ensure in advance that the probe (GNRs) is stable under this environment. We quantitatively analyzed the scattered light intensity from individual PEG protected GNRs when they were dispersed in DI water and in cell culture media for different time periods. As shown in Supporting Information Figure S5a, the width of the intensity distribution of GNRs dispersed in DI water was fairly narrow, indicating that the majority of the observed red spots are contributed by individual GNRs. The peak position of the scattering spectrum from these GNRs was 636 ± 13 nm. Figure S5b−d shows the intensity distribution of GNRs dispersed in cell culture media for 0, 14, and 24 h, respectively. These plots possess a similar peak width in comparison with that of GNRs dispersed in DI water. Moreover, the measured scattering maximum from GNRs dispersed in cell culture media is located at 640 ± 15 nm. This confirms that the GNRs used here are stable and are suitable for single-particle tracking experiments in living cells. Meanwhile, the high stability of these GNRs indicates that they could serve as promising drug, protein, and gene delivery cargos.

According to Chithrani's results,[37] gold nanoparticles suspended in cell culture media can spontaneously adsorb serum proteins onto their surfaces and enter the cell via a receptor-mediated endocytosis pathway. After co-incubating GNRs with HeLa cells for about 4 h, we could readily discriminate some red scattering spots within the cell region with comparable scattering intensity as that of individual GNRs immersed in cell culture medium. This indicates that the observed red spots inside the living cell are from individual GNRs and is consistent with Chithrani's experimental and Gao's theoretical results; that is, our individual GNRs fall into the favorable physical size range for the endocytosis pathway.[37,38]

Interestingly, we found that some GNRs diffused in the cytosol under a directed pathway toward the cell membrane. Previous reports have demonstrated that the active movement inside living cells can be ascribed to a motor-protein-assisted process.[23] Two types of motor proteins, dynein and kinesin, are involved in these processes. The kinesin protein delivers cargo toward the cell membrane, and dynein moves in the opposite direction.[39−42] Figure 4a shows a typical trajectory of a GNR diffusing toward the cell membrane with an interesting zigzag shape (see Movie 2 in the Supporting Information,). During the whole transport process, we could clearly see the GNR experiencing alternate pauses and forward steps as indicated in Figure 4b, depicting a motor-protein-assisted active transport process. Four unidirectional forward motions were observed with velocities of 0.47, 0.57, 0.64, and 0.67 μm/s at the intervals of 2.89−8.67, 10.84−12.53, 16.39−24.82, and 18.67−34.22 s, respectively. These values are comparable to the results of single kinesin

motor protein experiments inside living cells (0.60 μm/s).[43] So, most probably only one motor protein is involved in these processive intervals.

Although there are some detailed studies on the stepping mechanism of motor proteins on microtubules based on in vitro results, less is known about how they move inside living cells. Until now, several models (e.g., inchworm, asymmetric hand-over-hand, or hand-over-hand) have been developed to describe the walking behavior of individual kinesin proteins on microtubules.[44,45] In the inchworm region, it is assumed that the kinesin neck coil does not rotate 180° from the beginning of one step to the beginning of the next. If this assumption is applicable in vivo, the azimuthal angle of the GNR should not change when it is transported by kinesin protein on the microtubule provided the angle between the optical axis of birefringent prism and the long axis of the microtubule is fixed. A completely opposite observation would result according to the current hand-over-hand model where the two heads of kinesin protein alternate between adjacent steps. In other words, the neck coil would rotate 180° within each step. One of the most effective ways to resolve such rotational dynamics of motor proteins is to directly monitor the angle variation of anisotropic nanoparticles when they are transported by motor proteins.

From the measured polar angle of the GNR during the pausing and forward processes, we only observed small angle fluctuations, which was very different from the behavior of randomly diffusing GNRs in the cytosol. This shows that the observed GNR was firmly attached to the neck of kinesin protein but was not freely rotating inside the lysosome. This is in agreement with Louit's results[46] where the lipid layer of the lysosome is closely attached to the side wall of the gold nanoparticle. Through tracking of the azimuthal angle of the GNR in these processive intervals, we found that the angle of the GNR nearly kept constant except during the interval of 16.39−24.82 s (the residual angle variation in this interval can be attributed to angle variations of the path). The results presented here directly infer that the neck coil of kinesin does not rotate within each forward step in this case. Since the time resolution of our experiment is substantially lower than the time duration of each step, we cannot calculate directly the angle variation information step by step. However, our results could still discern whether the neck rotates with 180° within each step. Assuming the neck of kinesin rotates 180° within each individual step, we should observe evenly distributed scattering light from the X and Y channels when the exposure time is larger than the duration of each step. In other words, the measured angle should be 45° during the whole process, which is not the case for our in vivo results. In addition, we did not observe large variations in both the polar and azimuthal angles during the pausing intervals, revealing that the GNR was still firmly attached to the microtubule and did not diffuse away. These results further prove the reliability of the measured data during the processive intervals. Since we have no direct evidence to show that only one kinesin motor protein was involved in these forward processes, we cannot make a definitive conclusion on the stepping mechanism of individual kinesin motor proteins on microtubules in living cells. However, our method provides an excellent platform not only for three-dimensional angle determination but also for translational diffusion position measurement with high spatial and temporal resolution, especially if combined with laser illumination and a faster CCD camera.[22] The main limitation will be the bulkiness of the GNRs, which may affect the motion of the biomolecule. Therefore, further improvements in the detection sensitivity to allow the use of smaller GNRs will be valuable. Further experiments can be done by combining this method with, for example, controllably linking individual motor proteins on the side wall of GNRs and directly injecting them into the cytosol through osmotic lysis.[43]

CONCLUSION

In summary, the planar illumination method reported here provides an ideal solution to investigate translational and rotational motion of anisotropic nanoparticles as local order probes in heterogenerous nanoscopic environments. With this method, we directly monitored the rotational dynamics of individual GNRs dispersed in glycerol/water mixtures with different surface modifications. The measured rotational diffusion coefficient was well fitted to the TT model. In addition, the translational and rotational movements of an individual GNR transported by kinesin motor protein on microtubules inside living cells were directly imaged. From the in vivo results, we note that the observed motor-protein-loaded GNR did not rotate significantly during each forward step, which is similar to the in vitro results reported by Hua et al.[45] In comparison with the current strategies based on fluorescent dyes, our method provides much better optical stability for long time observations and potentially enables single-particle tracking with microsecond temporal resolution to capture transient events despite a noisy surrounding.

It should be noted that the planar illumination mode presented in this paper is just one optical scheme among many others that can detect 3D orientation of a single oscillating dipole. Because the light excitation probability function P_a and the detection probability function P_s are independent from each other, analyzing the scattering with orthogonal polarization detection with a small NA objective will give the azimuth angle of the dipole immediately regardless of the expression of P_a. The polar angle can then be derived from P_a as long as it is only related to the dipole orientation. Therefore, multiple illumination modes that include not only two-beam-planar but also one-beam-planar, axial, or one-beam-inclined illumination can all be utilized to obtain 3D orientation of a dipole while accommodating to the needs of different samples or microscopes, though only the two-beam-planar illumination mode can allow P_a reaching the highest value of 1 at all directions. Similarly, if only one unpolarized detector is used, the polar and azimuth angle of the dipole can also be determined by toggle either the polarization or direction of the excitation beam orthogonally at a rate faster than the rotational motion of the dipole. The expressions of P_a for some illumination/detection schemes that are commonly encountered or can be readily implemented are provided in the Supporting Information. These generalized planar illumination microscopy methods will greatly facilitate single anisotropic particle orientation studies and applications in various areas.

ASSOCIATED CONTENT

Supporting Information. Experimental procedures, additional figures, and movies as mentioned in the text. This material is available free of charge via the Internet at http://pubs.acs.org.

AUTHOR INFORMATION

Corresponding Author
yanhe2021@gmail.com

■ ACKNOWLEDGMENT

This work was supported by NSFC 20975036, NSFC 91027037, Program for New Century Excellent Talents in University, Program for Chang Jiang Scholars and Innovative Research Team in University and Hunan University 985 fund. L.-H. X. is thankful for partial support from Scholarship Award for Excellent Doctoral Student from Ministry of Education, China. E. S.Y. thanks the Ames Laboratory for partial support of this work.

■ REFERENCES

(1) Torre, J. G. d. l.; Martinez, M. C. L. *Macromolecules* **1987**, *20*, 661–666.
(2) Tirado, M. M.; Torre, J. G. d. l. *J. Chem. Phys.* **1980**, *73*, 1986–1993.
(3) Toprak, E.; Enderlein, J.; Syed, S.; McKinney, S. A.; Petschek, R. G.; Ha, T.; Goldman, Y. E.; Selvin, P. R. *Proc. Natl. Acad. Sci. U.S.A.* **2006**, *103*, 6495–6499.
(4) Vale, R. D.; Milligan, R. A. *Science* **2000**, *288*, 88–95.
(5) Bartko, A. P.; Xu, K.; Dickson, R. M. *Phys. Rev. Lett.* **2002**, *89*, 026101.
(6) Wöll, D.; Braeken, E.; Deres, A.; Schryver, F. C. D.; Uji-i, H.; Hofkens, J. *Chem. Soc. Rev.* **2009**, *38*, 313–328.
(7) Forkey, J. N.; Quinlan, M. E.; Goldman, Y. E. *Prog. Biophys. Mol. Biol.* **2000**, *74*, 1–35.
(8) Moerner, W. E.; Orrit, M. *Science* **1999**, *283*, 1670–1676.
(9) Yeung, E. S. *Annu. Rev. Anal. Chem.* **2004**, *55*, 97–126.
(10) Gould, T. J.; Gunewardene, M. S.; Gudheti, M. V.; Verkhusha, V. V.; Yin, S.-R.; Gosse, J. A.; Hess, S. T. *Nat. Methods* **2008**, *5*, 1027–1030.
(11) Harms, G. S.; Sonnleitner, M.; Schutz, G. J.; Gruber, H. J.; Schmidt, T. *Biophys. J.* **1999**, *77*, 2864–2870.
(12) Ha, T.; Laurence, T. A.; Chemla, D. S.; Weiss, S. *J. Phys. Chem. B* **1999**, *103*, 6839–6850.
(13) Nishizaka, T.; Oiwa, K.; Noji, H.; Kimura, S.; Muneyuki, E.; Yoshida, M.; Kinosita, K., Jr. *Nat. Struct. Mol. Biol.* **2004**, *11*, 142–148.
(14) Ha, T.; Glass, J.; Enderle, T.; Chemla, D. S.; Weiss, S. *Phys. Rev. Lett.* **1998**, *80*, 2093–2096.
(15) Ha, T.; Enderle, T.; Chemla, D. S.; Selvin, P. R.; Weiss, S. *Phys. Rev. Lett.* **1996**, *77*, 3979–3982.
(16) Tsay, J. M.; Doose, S.; Weiss, S. *J. Am. Chem. Soc.* **2006**, *128*, 1639–1647.
(17) Derfus, A. M.; Chan, W. C. W.; Bhatia, S. N. *Nano Lett.* **2004**, *4*, 11–18.
(18) Kelly, K. L.; Coronado, E.; Zhao, L. L.; Schatz, G. C. *J. Phys. Chem. B* **2003**, *107*, 668–677.
(19) Jain, P. K.; Huang, X.; El-Sayed, I. H.; El-Sayed, M. A. *Acc. Chem. Res.* **2008**, *41*, 1578–1586.
(20) Xiao, L.; Wei, L.; He, Y.; Yeung, E. S. *Anal. Chem.* **2010**, *82*, 6308–6314.
(21) Jain, P. K.; Lee, K.-S.; H.El-Sayed, I.; El-Sayed, M. A. *J. Phys. Chem. B* **2006**, *110*, 7238–7248.
(22) Noda, N.; Kamimura, S. *Rev. Sci. Instrum.* **2008**, *79*, 023704.
(23) Nan, X.; Sims, P. A.; Xie, X. S. *ChemPhysChem* **2008**, *9*, 707–712.
(24) Spetzler, D.; York, J.; Daniel, D.; Fromme, R.; Lowry, D.; Frasch, W. *Biochemistry* **2006**, *45*, 3117–3124.
(25) Sau, T. K.; Murphy, C. J. *Langmuir* **2004**, *20*, 6414–6420.
(26) Sönnichsen, C.; T. Franzl, T. W.; Plessen, G. v.; Feldmann, J.; Wilson, O.; Mulvaney, P. *Phys. Rev. Lett.* **2002**, *88*, 077402.
(27) Sonnichsen, C.; Alivisatos, A. P. *Nano Lett.* **2005**, *5*, 301–304.
(28) Chang, W.-S.; Haa, J. W.; Slaughter, L. S.; Link, S. *Proc. Natl. Acad. Sci. U.S.A.* **2010**, *107*, 2781–2786.
(29) Failla, A. V.; Qian, H.; Qian, H.; Hartschuh, A.; Meixner, A. J. *Nano Lett.* **2006**, *6*, 1374–1378.
(30) Xiao, L.; Qiao, Y.; He, Y.; Yeung, E. S. *Anal. Chem.* **2010**, *82*, 5268–5274.
(31) Wang, G.; Sun, W.; Luo, Y.; Fang, N. *J. Am. Chem. Soc.* **2010**, *132*, 16417–16422.
(32) Xiao, L.; He, Y.; Yeung, E. S. *J. Phys. Chem. C* **2009**, *113*, 5991–5997.
(33) Axelrod, D. *Biophys. J.* **1979**, *26*, 557–574.
(34) Bhaduri, B.; Neild, A.; Ng, T. W. *Appl. Phys. Lett.* **2008**, *92*, 084105.
(35) Angelo, S. K. S.; Waraksa, C. C.; Mallouk, T. E. *Adv. Mater.* **2003**, *15*, 400–402.
(36) Pierrat, S.; Hartinger, E.; Faiss, S.; Janshoff, A.; Sonnichsen, C. *J. Phys. Chem. C* **2009**, *113*, 11179–11183.
(37) Chithrani, B. D.; Ghazani, A. A.; Chan, W. C. W. *Nano Lett.* **2006**, *6*, 662–668.
(38) Gao, H.; Shi, W.; Freund, L. B. *Proc. Natl. Acad. Sci. U.S.A.* **2005**, *102*, 9469–9474.
(39) Valetti, C.; Wetzel, D. M.; Schrader, M.; Hasbani, M. J.; Gill, S. R.; Kreis, T. E.; Schroer, T. A. *Mol. Biol. Cell* **1999**, *10*, 4107–4120.
(40) Hirokawa, N. *Science* **1998**, *279*, 519–526.
(41) Burkhardt, J. K.; Echeverri, C. J.; Nilsson, T.; Vallee, R. B. *J. Cell Biol.* **1997**, *139*, 469–484.
(42) Hollenbeck, P. J.; Swanson, J. A. *Nature* **1990**, *346*, 864–866.
(43) Courty, S.; Luccardini, C.; Bellaiche, Y.; Cappello, G.; Dahan, M. *Nano Lett.* **2006**, *6*, 1491–1495.
(44) Yildiz, A.; Forkey, J. N.; McKinney, S. A.; Ha, T.; Goldman, Y. E.; Selvin, P. R. *Science* **2003**, *300*, 2061–2065.
(45) Hua, W.; Chung, J.; Gelles, J. *Science* **2002**, *295*, 844–848.
(46) Louit, G.; Asahi, T.; Tanaka, G.; Uwada, T.; Masuhara, H. *J. Phys. Chem. C* **2009**, *113*, 11766–11772.